

Generative Predictive Control: Flow Matching Policies for Dynamic, Difficult-to-Demonstrate Tasks

Vince Kurtz

Civil and Mechanical Engineering
California Institute of Technology
vkurtz@caltech.edu

Joel W. Burdick

Civil and Mechanical Engineering
California Institute of Technology
jwb@robotics.caltech.edu

Abstract: Generative control policies have recently unlocked major progress in robotics. These methods produce action sequences via diffusion or flow matching, with training data provided by demonstrations. But existing methods come with two key limitations: they require expert demonstrations, which can be difficult to obtain, and they are limited to relatively slow, quasi-static tasks. In this paper, we leverage a tight connection between sampling-based predictive control and generative modeling to address each of these issues. In particular, we introduce *generative predictive control*, a supervised learning framework for tasks with fast dynamics that are easy to simulate but difficult to demonstrate. We then show how trained flow-matching policies can be warm-started at inference time, maintaining temporal consistency and enabling high-frequency feedback. We believe that generative predictive control offers a complementary approach to existing behavior cloning methods, and hope that it paves the way toward generalist policies that extend beyond quasi-static demonstration-oriented tasks.

Keywords: Generative models, flow matching, sampling-based predictive control

1 Introduction and Related Work

Diffusion and flow matching policies have enabled tremendous success in behavior cloning for quasi-static manipulation [1, 2, 3, 4]. Can generative policies also control systems with fast nonlinear dynamics at high control frequencies, where demonstrations are difficult to come by? In this paper, we answer this question in the affirmative by introducing generative predictive control (GPC), a supervised learning framework for dynamic and difficult-to-demonstrate tasks.

Fig. 1 summarizes our approach. GPC alternates between data collection via sampling-based predictive control (SPC) and policy training via flow matching. The flow model provides extra samples for SPC, enabling continual performance improvement while maintaining a supervised (regression) objective.

Generative Policies: Diffusion [1] and flow matching [2] have recently gained prominence as powerful policy representations for robotics. These models typically focus on behavior cloning [3, 4], where expert demonstrations serve as training data. Generative policies have the key advantage of multi-modal expressiveness, allowing multiple “paths” to the same goal [1]. They also provide a natural choice for handling image data [11, 12, 13].

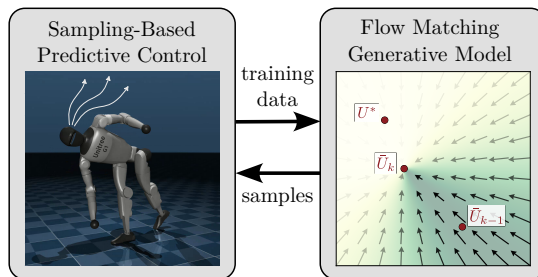


Figure 1: Generative predictive control is a supervised learning framework for dynamic tasks that are difficult to demonstrate but easy to simulate. First, we generate training data with sampling-based predictive control [5, 6, 7], leveraging advances in massively parallel GPU simulation [8, 9, 10]. We then use this data to train a flow matching policy, which in turn provides additional high-quality samples. This results in better training data for subsequent iterations, in a virtuous cycle.

Importantly, generative policies are trained in a *supervised* manner, with clearly defined regression targets. This improves training stability over unsupervised reinforcement learning [14, 15], but requires demonstrations. Obtaining sufficient demonstration data is a key challenge, particularly for large generalist policies [2, 16, 17]. While creative ways to obtain this data are an area of active research [18], it is unlikely that demonstrations alone will produce the internet-scale data used to train large vision-language models any time soon. Furthermore, some tasks are simply difficult to demonstrate, particularly for robots with fast nonlinear dynamics or unique morphologies.

Sampling-based Predictive Control (SPC): At the same time, a very different trend has been gaining traction in the nonlinear optimal control community. SPC is an alternative to gradient-based model predictive control (MPC), where a simple sampling procedure is used in place of a sophisticated nonlinear optimizer [19, 20, 21]. Algorithms in this family include model predictive path integral control (MPPI) [6], predictive sampling (PS) [7], and cross-entropy methods (CEM) [22]. SPC algorithms are exceedingly easy to implement, and have been studied for a long time. But recent advances in computing speed and parallel simulation [8, 9, 10] have enabled them to scale to complex problems like in-hand dexterous manipulation [5], legged locomotion [23] and more [24, 7].

In many ways, SPC is complementary to generative behavior cloning: it is agnostic to a robot’s morphology, and can be particularly effective on tasks with fast nonlinear dynamics. Behavior cloning, on the other hand, has shown particular success on tasks involving deformable objects like cloth and food [1, 2, 3, 4], which are difficult to simulate at speeds sufficient for SPC.

Our Contributions: In this paper, we highlight a surprisingly deep connection between generative policies and SPC. This connection was first identified by [25] in the context of MPPI: here we extend this connection to a general class of SPC algorithms.

We then leverage this connection to propose a supervised learning framework for difficult-to-demonstrate tasks, GPC. We show how flow-matching policies can be warm-started to encourage temporal consistency, and demonstrate that these warm-starts are critical for high-frequency feedback. To push the scalability limits of GPC, we train policies on systems ranging from a simple inverted pendulum to a humanoid robot, and evaluate effectiveness in simulation. Our largest and most difficult task (humanoid standup) exposes these scalability limits: seeding SPC with a GPC policy is effective, but applying the policy directly is not. With this in mind, we provide an extensive discussion of limitations and directions for future work.

2 Background

In this paper we consider optimal control problems of the standard form

$$\min_{u_0, u_1, \dots, u_T} \phi(x_{T+1}) + \sum_{\tau=0}^T \ell(x_\tau, u_\tau), \quad (1a)$$

$$\text{s.t. } x_{\tau+1} = f(x_\tau, u_\tau), \quad (1b)$$

$$x_0 = x_{init}, \quad (1c)$$

where $x_\tau \in \mathbb{R}^n$ represents the system state at time step τ , $u_\tau \in \mathbb{R}^m$ are control actions, $\ell(\cdot, \cdot)$ and $\phi(\cdot)$ are running and terminal costs, and $f(\cdot, \cdot)$ captures the system dynamics. For simplicity, we denote the T -length action sequence as $U = [u_0, u_1, \dots, u_T]$ and rewrite (1) in compact form as

$$\min_U J(U; x_{init}), \quad (2)$$

where both the costs and dynamics constraints are wrapped into the (highly non-convex) objective.

2.1 Sampling-based Predictive Control

MPC methods traditionally solve (1) with gradient-based non-convex optimization. But these techniques face significant challenges, particularly when it comes to the stiff and highly nonlinear contact dynamics essential for contact-rich robot locomotion and manipulation [26, 19, 20, 21].

In response to these challenges, SPC is gaining prominence as a simple and computationally efficient alternative to gradient-based MPC [5, 6, 23, 27, 28]. Instead of relying on the complex machinery of nonlinear optimization, SPC algorithms perform some variation on the following simple procedure:

1. At step k , sample N candidate action sequences from a Gaussian proposal distribution¹.

$$U^{(i)} \sim \mathcal{N}(\bar{U}_{k-1}, \sigma^2), \quad i \in [1, N]. \quad (3)$$

2. Roll out each action sequence from the latest state estimate x_{k-1} , recording the costs

$$J^{(i)} = J(U^{(i)}; x_{k-1}). \quad (4)$$

3. Update the mean action sequence according to some weighting function $g: \mathbb{R} \rightarrow \mathbb{R}^+$,

$$\bar{U}_k = \bar{U}_{k-1} + \frac{\sum_{i=1}^N g(J^{(i)})(U^{(i)} - \bar{U}_{k-1})}{\sum_{i=1}^N g(J^{(i)})}. \quad (5)$$

4. Apply the first action from \bar{U}_k , and repeat in MPC fashion from the updated state x_k .

The weighting function g distinguishes different SPC algorithms. As detailed in Appendix A, different choices give rise to MPPI [6], predictive sampling [7], CEM [22, 5], and more [29].

The ability to parallelize rollouts (4) is a key advantage over gradient-based MPC. The advent of massively parallel GPU simulators [8, 9, 10] further reinforces this advantage. Sampling can also reduce the severity of local minima and smooth out stiff dynamics associated with contact [30, 31].

2.2 Generative Modeling

Generative modeling considers a seemingly very different problem: produce a sample \mathbf{x} from a probability distribution $p(\mathbf{x})$. In the typical setting, we do not have access to $p(\mathbf{x})$ in closed form, but we do have samples (training data) from this data distribution.

Flow Matching: Flow matching [13] is based on the idea of a *probability density path* $p_t(\mathbf{x})$. This path flows from an easy-to-sample distribution $p_0(\mathbf{x}) = \mathcal{N}(0, I)$ at $t = 0$ to the data distribution at $t = 1$. Flow matching methods learn a vector field $v_\theta(\mathbf{x}, t)$ that moves samples along this path.

The flow network v_θ is trained via standard (stochastic) gradient descent methods on

$$\min_{\theta} \mathbb{E}_{t, \mathbf{x}_0, \mathbf{x}_1} [\mathcal{L}_{FM}(\theta; \mathbf{x}_0, \mathbf{x}_1, t)], \quad (6)$$

where θ are learnable parameters (e.g., network weights and biases) and

$$\mathcal{L}_{FM}(\theta; \mathbf{x}_0, \mathbf{x}_1, t) = \|v_\theta(t\mathbf{x}_1 + (1-t)\mathbf{x}_0, t) - (\mathbf{x}_1 - \mathbf{x}_0)\|^2. \quad (7)$$

The expectation in (6) is taken over $t \sim \mathcal{U}(0, 1)$, $\mathbf{x}_0 \sim p_0(\mathbf{x})$, and $\mathbf{x}_1 \sim p_1(\mathbf{x})$. Each of these are easy to sample, since we already have data points \mathbf{x}_1 , and sampling $p_0(\mathbf{x})$ is trivial. Intuitively, \mathcal{L}_{FM} pushes samples in a straight line from \mathbf{x}_0 to \mathbf{x}_1 . At inference time, we first sample $\mathbf{x} \sim p_0(\mathbf{x})$, then integrate $\dot{\mathbf{x}} = v_\theta(\mathbf{x}, t)$ from $t = 0$ to $t = 1$, typically with a simple explicit Euler scheme.

Diffusion: Flow matching is equivalent (under some technical conditions [32]) to diffusion-based generative modeling [11, 12]. Diffusion models also consider a series of probability distributions flowing from an initial Gaussian to the data distribution. But rather than being parameterized by a time t , these are typically parameterized by additive noise σ ,

$$p_\sigma(\mathbf{x}) = \int p(\mathbf{y}) \mathcal{N}(\mathbf{x}; \mathbf{y}, \sigma^2 I) d\mathbf{y}. \quad (8)$$

For large σ , $p_\sigma(\mathbf{x})$ approaches an easy-to-sample Gaussian. For small σ , $p_\sigma(\mathbf{x})$ approaches $p(\mathbf{x})$.

Diffusion models learn the score $s_\theta(\mathbf{x}, \sigma) \approx \nabla_{\mathbf{x}} \log p_\sigma(\mathbf{x})$ by removing noise added to the original data [11, 12]. We can then use s_θ to sample from p_σ using Langevin dynamics

$$\mathbf{x} \leftarrow \mathbf{x} + \epsilon s_\theta(\mathbf{x}, \sigma) + \sqrt{2\epsilon} \mathbf{z} \quad \mathbf{z} \sim \mathcal{N}(0, I), \quad (9)$$

with step size $\epsilon > 0$. By gradually reducing σ , we arrive at samples from the data distribution $p(\mathbf{x})$.

¹Some SPC methods use a non-isotropic proposal distribution and update the variance of the proposal distribution along with the mean. We focus on an isotropic Gaussian with fixed variance for simplicity.

3 SPC is Online Generative Modeling

In this section, we establish a formal connection between SPC and generative modeling. Specifically, we show that the SPC update (5) is a Monte Carlo estimate of the score of a noised target distribution. This connection was first identified for the case of MPPI in [25] and used to develop Dial-MPC, a multi-stage SPC algorithm for legged locomotion [23]. Here we extend this connection to generic SPC algorithms with updates of the form (5).

First, we define a target distribution conditioned on the initial state x :

$$p(U | x) \propto g(J(U; x)), \quad (10)$$

which is determined by the algorithm-specific weighting function $g(\cdot)$ introduced in Sec. 2.1 above. In the spirit of score-based diffusion [12] we define the noised target distribution

$$p_\sigma(U | x) \propto \mathbb{E}_{\tilde{U} \sim \mathcal{N}(U, \sigma^2)} [g(\tilde{U})]. \quad (11)$$

It turns out the score of this noised target is directly related to the SPC update (5):

Proposition 1. *The score of the noised target distribution (11) is given by*

$$\nabla_U \log p_\sigma(U | x) = \frac{1}{\sigma^2} \frac{\mathbb{E}_{\tilde{U} \sim \mathcal{N}(U, \sigma^2)} [g(\tilde{U})(\tilde{U} - U)]}{\mathbb{E}_{\tilde{U} \sim \mathcal{N}(U, \sigma^2)} [g(\tilde{U})]}. \quad (12)$$

This means that the SPC update (5) provides a Monte-Carlo estimate of score ascent, e.g.,

$$\bar{U}_k \leftarrow \bar{U}_{k-1} + \sigma^2 \nabla_{\bar{U}_{k-1}} \log p_\sigma(\bar{U}_{k-1} | x_{k-1}) \quad (13)$$

The additional σ^2 term may seem like a troublesome annoyance, but in fact Langevin step sizes $\epsilon \propto \sigma^2$ are a standard recommendation in the diffusion literature [11, Algorithm 1]. Here, this choice of step size emerges naturally from the SPC update (5).

This connection also sheds light on the benefits of predictive sampling (where we merely choose the best sample) [7]. In particular, the un-noised target distribution for predictive sampling is a dirac delta concentrating all probability mass at the globally optimal solution [25, Appendix A], leading to a noised target distribution $p_\sigma(U | x)$ with a single mode at the globally optimal solution. In this sense, **predictive sampling approximates generative modeling for a distribution with a single mode at the global optimum**. For this reason, we focus our numerical investigations primarily on predictive sampling. A more thorough theoretical exploration of the advantages and disadvantages of other SPC algorithms is an important topic for future work.

4 Generative Predictive Control

The previous section shows that we can think of the mean of the SPC sampling distribution, \tilde{U}_k , as being drawn from the state-conditioned optimal action distribution

$$\bar{U}_k \sim p(U | x_k) \propto g(J(U; x_k)). \quad (14)$$

This leads to a natural question: can we train a generative model to produce \bar{U}_k directly? In addition to imitating the SPC update process, such a generative model

$$p_\theta(U | x_k) \approx p(U | x_k), \quad (15)$$

parameterized by network weights θ , would maintain a structure compatible to the flow matching and diffusion models used in behavior cloning [1, 4, 3, 2].

Remark 1. *Behavior cloning methods condition on observations $y = h(x)$ (or a history of such observations) rather than a full state estimate [1]. While we write $p_\theta(U | x)$ for notational simplicity, the GPC framework can also be applied to observation conditioning. In fact, our implementation uses observations $h(x)$ rather than the full state x , as detailed in Appendix E.*

This is the basic idea behind GPC. We use data (\bar{U}_k, x_k) from running SPC in simulation to train a flow matching model (15). This model is characterized by a vector field

$$\dot{U} = v_\theta(U, x, t) \quad (16)$$

that pushes samples from $U_t \sim \mathcal{N}(0, I)$ at $t = 0$ to the target distribution (14) at $t = 1$. To learn this vector field, we minimize a conditional flow matching loss similar to (6),

$$\mathcal{L}_{GPC}(\theta; U_0, \bar{U}_k, x_k, t) = \|v_\theta(t\bar{U}_k - (1-t)U_0, x_k, t) - (\bar{U}_k - U_0)\|^2, \quad (17)$$

where (\bar{U}_k, x_k) are data points generated by the SPC controller, $U_0 \sim \mathcal{N}(0, I)$ is a sample from the proposal distribution, and $t \sim \mathcal{U}(0, 1)$ is sampled uniformly along the probability path.

To further improve training efficiency, we weigh data points according to cosine similarity with $\bar{U}_k - \bar{U}_{k-1}$. This puts greater emphasis on samples similar to \bar{U}_{k-1} , as illustrated by the shading in Fig. 1. Further details can be found in Appendix C.

However, **directly training a generative model on SPC data is not particularly effective**, as the training targets are very noisy [33]. To avoid this issue, GPC performs several cycles of SPC simulation and model fitting. This is illustrated in Fig. 1 and outlined in Algorithm 1. In each cycle, samples from the partially-trained flow matching policy are used to bootstrap SPC, providing an improved sampling distribution and thus better training data for the next model fitting step.

Algorithm 1: Generative Predictive Control

Input: SPC algorithm $g(U)$, flow matching model $p_\theta(U | x)$, system model $f(x, u)$.

Output: Trained flow model parameters θ .

```

1 while not converged do
2   for  $j = 1, \dots, N_E$  do
3      $x_0^{(j)} \sim \mathcal{X}_0$  // Sample initial conditions in parallel environments
4      $\bar{U}_0^{(j)} \sim \mathcal{N}(0, \sigma^2 I)$ 
5     for  $k \in [1, K]$  do
6        $U^{(i,j)} \sim \mathcal{N}(\bar{U}_{k-1}^{(j)}, \sigma^2 I)$ ,  $i \in [1, N_S]$  // Sample action sequences
7        $U^{(i,j)} \sim p_\theta(\bar{U}_{k-1}^{(j)} | x_{k-1}^{(j)})$ ,  $i \in [N_S, N]$ 
8        $J^{(i,j)} \leftarrow J(U^{(i,j)}; x_{k-1}^{(j)})$  // Parallel rollouts
9        $\bar{U}_k^{(j)} \leftarrow \bar{U}_{k-1}^{(j)} + \frac{\sum_{i=1}^N g(J^{(i,j)})(U^{(i,j)} - \bar{U}_{k-1}^{(j)})}{\sum_{i=1}^N g(J^{(i,j)})}$  // Update actions via SPC
10       $x_k^{(j)} \leftarrow f(x_{k-1}^{(j)}, u_k^{(j)})$  // Advance the simulations
11    end
12  end
13   $\theta \leftarrow \arg \min_\theta \mathbb{E}_{t, U_0, j, k} [\mathcal{L}_{GPC}(\theta; U_0, \bar{U}_k^{(j)}, \bar{U}_{k-1}^{(j)}, x_k^{(j)}, t)]$  // Fit flow model
14 end
```

We first sample initial states $x_0^{(j)}$ from initial conditions \mathcal{X}_0 for N_E parallel simulation environments. We then proceed to perform SPC in each environment, with N_S of the samples coming from the typical Gaussian proposal distribution (line 6) and the remaining samples from the flow matching policy (line 7). The policy samples help improve performance, while the Gaussian samples prevent distribution collapse. After collecting a dataset of states $x_k^{(j)}$ and action sequences $U_k^{(j)}$, we fit the flow matching model (line 13). The expectation in this case is over flow timesteps $t \in \mathcal{U}(0, 1)$, initial samples $U_0 \sim \mathcal{N}(0, I)$, parallel environments $j = 1, \dots, N_E$, and simulation steps $k = 1, \dots, K$.

GPC benefits from parallelism throughout Algorithm 1. In addition to parallel rollouts in the SPC update step (line 8), we parallelize over simulation environments (line 2) and in the model training step (line 13). Our implementation leverages the vectorization and parallelization tools in JAX [34] together with the massively parallel robotics simulation made possible by MuJoCo MJX [8].

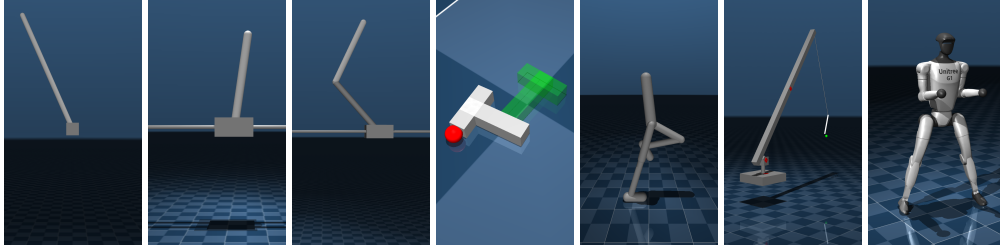


Figure 2: Systems used to evaluate GPC performance in simulation, from left to right: inverted pendulum, cart-pole, double cart-pole, push-T, planar walker, luffing crane, humanoid standup.

5 Using a Trained GPC Policy

Warm-starts: In fast feedback loops, the multi-modal expressiveness of generative models presents a challenge: samples at subsequent timesteps can be drawn from different modes, leading to “jittering” behavior. This is known as *temporal consistency* [3]. A common solution is to roll out several steps of the action sequence before replanning [1]. This forces the controller to “commit” to a particular mode, but is not suitable for highly dynamic tasks. Other alternatives include averaging over samples produced at different timesteps [3], but this is not always effective in practice [2].

We propose a simple alternative inspired by warm-starts in MPC. Rather than starting the flow generation process from $U_0 \sim \mathcal{N}(0, I)$, we start from

$$U_0 = (1 - \alpha)\mathcal{N}(0, I) + \alpha\bar{U}_{k-1} \quad (18)$$

where $\alpha \in [0, 1]$ is the *warm-start level*. With $\alpha = 1$, the flow process is started from the previous sample \bar{U}_{k-1} , while $\alpha = 0$ recovers the Gaussian proposal distribution. Because flow matching defines a vector field that drives samples toward a mode of the sampling distribution, flows with a high warm-start level α tend to stay close to the same mode as the previous sample, \bar{U}_{k-1} . We find that this simple warm-start procedure enables smooth and performant high-frequency control.

Deploying the policy: There are two ways we might use a GPC policy. The first is to deploy the policy directly, applying actions in receding-horizon fashion, possibly with warm-starts. We refer to this strategy as simply *GPC*. The second is to use policy samples for SPC, alongside samples from the usual Gaussian proposal distribution. We refer to this bootstrapping approach as *GPC+*. **GPC+ leverages inference-time compute for better performance**, but requires a state estimate from which to perform the rollouts. Ordinary GPC does not require a state estimate, as the policy can be conditioned on arbitrary observations (Remark 1).

Risk-Aware Domain Randomization: Domain (DR) has emerged as a key ingredient in enabling sim-to-real transfer of policies trained in simulation, particularly for reinforcement learning [35, 36]. It is reasonable to expect that DR will also play a critical role in sim-to-real transfer of GPC policies.

Interestingly, the advent of massively parallel simulators and the structure of the SPC/GPC paradigm enables a range of new DR possibilities. In particular, we can consider a whole family of DR strategies ranging from simple average-case robustness to more sophisticated risk metrics like conditional value-at-risk (CVar) [37, 38]. These strategies are detailed in Appendix D.

6 Simulation Studies

In this section, we consider the seven test systems shown in Fig. 2. We aim to answer the following:

1. Can GPC perform tasks that require multi-modal reasoning, as well highly dynamic tasks that require high-frequency feedback (Sec. 6.1)?
2. Does GPC continually improve policy performance over multiple iterations (Sec. 6.2)?
3. How do different domain randomization strategies impact performance (Sec. 6.3)?
4. What are the scalability limits of this approach (Sec. 6.4)?

In short, GPC is effective for control systems with fast dynamics at high feedback rates, enjoys the training stability characteristic of supervised learning methods, and enables risk-aware control, but struggles to scale to our largest and most difficult example (humanoid standup). We provide further discussion of these scalability limits, and how they might be overcome, in the limitations section.

We test GPC on seven simulated systems of varying state dimension and task difficulty, shown in Fig. 2. The *pendulum*, *cart-pole*, and *double cart-pole* are tasked with balancing upright. In *push-T*, an actuated finger pushes a block to a goal pose. The *walker* aims to move forward at a constant velocity, while the *crane* swings its payload to a target position. The *humanoid* attempts to stand up from arbitrary initial configurations. Further details can be found in Appendix E.

The smaller examples use a simple multi-layer perceptron for the flow network v_θ , while the larger examples use a convolutional network with FiLM conditioning [39], as recommended in [1]. All experiments were performed on a desktop computer with an NVIDIA RTX 4070 (12 GB) GPU. When evaluating trained policies, we use MuJoCo CPU rather than MJX.

6.1 Policy Performance

Footage of closed-loop GPC performance on each of the examples is shown in the accompanying video [40]. To evaluate performance quantitatively, we perform 100 simulations of SPC, GPC, and GPC+ from random initial conditions and record the average cost per time step (Fig. 4). GPC inference times range between 1 and 10 milliseconds, enabling feedback rates between 100-1000 Hz. Fig. 4 provides some insight into relative performance, but does not capture the full picture. For instance, on the walker we find that GPC enables smoother actions with far less “stumbling” than SPC, though cost per step indicates similar performance.

We find that **GPC can handle multi-modal action distributions**. This is evidenced by effectiveness on the push-T, which requires multi-modal reasoning to reach around the block [1]. Interestingly, GPC training takes under 20 minutes, while training a similar diffusion policy (with full state observations) takes around an hour, not counting the time to gather demonstrations [1].

More importantly, **GPC can control systems with fast dynamics at high control rates**. The double cart-pole provides a particularly clear illustration of this fact, as well as the importance of warm-starts. Fig. 3 shows performance with and without warm-starts. Without warm-starts (left, $\alpha = 0$), the control actions are dominated by significant noise (top plot) and the system is unable to swing upright (bottom plot). With warm-starts (right, $\alpha = 1$), we obtain smoother control actions and the robot successfully balances around the upright configuration. The controller is still able to respond rapidly to the chaotic system dynamics, as evidenced by the rapid changes between 1 and 2 seconds.

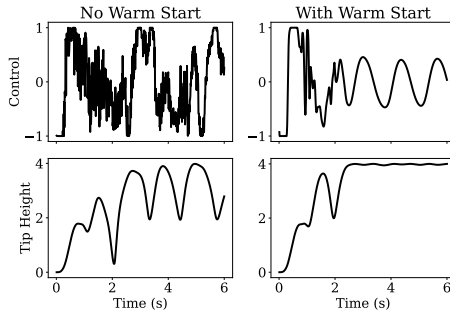


Figure 3: Closed-loop double cart-pole performance with and without warm-starts. The warm-started policy (right) produces smooth actions and is able to successfully balance. Without warm-starts (left), actions jitter between modes, and the robot fails to balance.

6.2 Training Stability

During training process, we find that average cost of policy samples decreases monotonically between iterations, modulo noise from initial conditions. This indicates that GPC’s cycle of training and sampling does continually improve performance. These and other training curves are available in Appendix F. While we leave a systematic hyperparameter sensitivity study for future work, our empirical observation is that **GPC benefits from the training stability of supervised learning**. This is in contrast to reinforcement learning methods, which can exhibit high sensitivity to reward tuning, implementation details, and even the random seed used for training [15, 14].

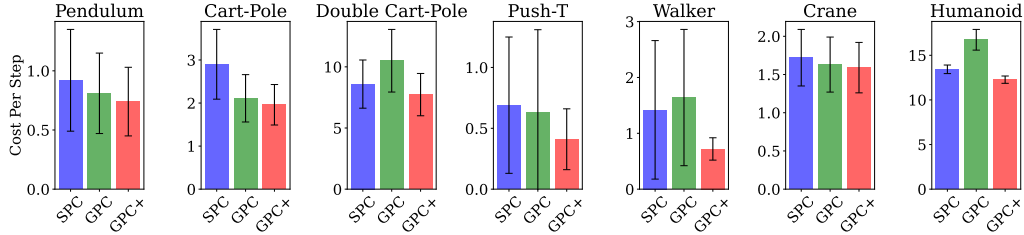


Figure 4: Average cost per time step for SPC, GPC (policy alone), and GPC+ (policy + sampling). Black bars indicate standard deviation over 100 ten-second simulations from randomized initial conditions. Applying the GPC policy directly provides performance on-par-with or better-than SPC in all cases except humanoid standup. GPC+ meets or exceeds the performance of the other methods across all examples.

6.3 Risk-Aware Domain Randomization

We use the luffing crane example to explore the impact of different DR strategies. Specifically, we train three GPC policies: one with no DR, one with standard average-cost DR, and one with a more conservative CVaR(0.25) strategy. We use 8 randomized domains, each with slightly different joint damping, payload mass, payload inertia, and actuator gains.

	No DR	Avg.	CVaR
No model error	106	103	133
With model error	165	184	139

Table 1: Time (seconds) for the crane to visit a sequence of 50 randomly generated payload targets, under policies trained without DR (“No DR”), with standard DR (“Avg.”), and with a risk-averse strategy (“CVaR”). CVaR improves robustness to model error, at the cost of worse performance under nominal conditions.

After training, we apply GPC directly with warm-starts. To evaluate closed-loop performance, we generate 50 random target locations that the payload must visit. The target is moved to the next location once the payload is moved within 15 cm or after 10 seconds, whichever comes first. Table 1 reports the total time to visit all 50 targets: lower times indicate better performance. The same sequence of target locations are used for each policy.

Without model error in the simulator, both the non-randomized policy and average-case DR perform significantly better than the more conservative CVaR policy. When we add model error to the simulator (lower joint damping, heavier payload mass), all methods perform worse. But the more conservative CVaR policy degrades the least, and significantly outperforms the others.

6.4 Scalability

In choosing our set of example systems, which range from 1 to 29 degrees-of-freedom, we aim to find the scalability limits of Algorithm 1. This **scalability hits a bottleneck with the largest humanoid example**: the GPC policy alone is unable to reliably stand up, though GPC+ is effective.

It is likely that further cost and hyperparameter tuning, curriculum training, and more computation could improve performance for the humanoid example. However, state-of-the-art reinforcement learning methods are able to train similar behaviors [41, 42], suggesting that further algorithmic improvements in the GPC framework are necessary to achieve reliable scalability to such systems.

7 Conclusion

We introduced generative predictive control (GPC), a framework for learning flow matching policies on dynamic tasks that are easy to simulate but difficult to demonstrate. GPC leverages tight connections between generative modeling and sampling-based predictive control to generate training data for supervised learning without expert demonstrations. We showed how warm-started GPC policies enable real-time high-frequency control, ensuring temporal consistency via warm-starts. Future work will focus on validating the GPC framework on hardware, incorporating value function learning, and training generalist multi-task policies.

Limitations

Limited effectiveness on our largest (humanoid standup) example is the most severe limitation of our proposed method, as noted above. We believe that **value function learning will be a critical component in overcoming this limitation**. In addition to being a key element of state-of-the-art reinforcement learning methods, value learning would allow us to reduce the planning horizon T in Problem 1. Reducing the planning horizon reduces the dimensionality of the sampling space, making planning easier while maintaining long-horizon reasoning. Methods that leverage connections between the gradient of the value function and the flow field v_θ —which is closely related to the score $\nabla \log p(U | x)$ and therefore the gradient of the cost (2)—are of particular interest.

For the basic GPC framework introduced here, sample complexity is relatively poor: to generate a single training data point, we run N short simulations—and even more under a risk-aware DR strategy. While advances in computing speeds may mean that the benefits of a supervised learning framework eventually outweigh the computational costs, methods of more fully using *all* of the data from SPC rollouts could significantly improve the GPC framework.

Other performance improvements could come from more benign algorithmic details. For instance, we represent action sequences with a simple zero-order-hold spline parameterization. Higher-order splines [7] or alternative parameterizations could be more effective. Better choices of action space, such as using task-space/end-effector coordinates rather than joint coordinates, could also be useful. Actuation limits are a critical component of many robotics tasks, but our implementation does not handle these in any particularly special way. Leveraging recent advances in constrained generative modeling [43, 44, 45] to do so is another potentially fruitful area for future work.

Future work will include evaluating GPC on hardware. Hardware experiments are a critical for evaluating any robot control framework: this is particularly the case when it comes to domain randomization strategies. Hardware experiments will also provide an important platform for exploring policies conditioned on various observations, ranging from raw sensor data to images to foundation model embeddings [46]. Integrated simulation and rendering in the recently-released MuJoCo playground [47] could provide a useful software platform for training image-conditioned policies.

Finally, the GPC framework offers a path toward including dynamic and difficult-to-demonstrate tasks in a generalist policy or large behavior model that combines data from many tasks [2, 16, 17]. Exploring this possibility remains an important topic for future work.

References

- [1] C. Chi, S. Feng, Y. Du, Z. Xu, E. Cousineau, B. Burchfiel, and S. Song. Diffusion policy: Visuomotor policy learning via action diffusion. *arXiv preprint arXiv:2303.04137*, 2023.
- [2] K. Black, N. Brown, D. Driess, A. Esmail, M. Equi, C. Finn, N. Fusai, L. Groom, K. Hausman, B. Ichter, et al. π_0 : A vision-language-action flow model for general robot control. *arXiv preprint arXiv:2410.24164*, 2024.
- [3] T. Z. Zhao, V. Kumar, S. Levine, and C. Finn. Learning fine-grained bimanual manipulation with low-cost hardware. *arXiv preprint arXiv:2304.13705*, 2023.
- [4] Z. Fu, T. Z. Zhao, and C. Finn. Mobile aloha: Learning bimanual mobile manipulation using low-cost whole-body teleoperation. In *8th Annual Conference on Robot Learning*.
- [5] A. H. Li, P. Culbertson, V. Kurtz, and A. D. Ames. Drop: Dexterous reorientation via online planning. *arXiv preprint arXiv:2409.14562*, 2024.
- [6] G. Williams, P. Drews, B. Goldfain, J. M. Rehg, and E. A. Theodorou. Aggressive driving with model predictive path integral control. In *2016 IEEE International Conference on Robotics and Automation (ICRA)*, pages 1433–1440. IEEE, 2016.
- [7] T. Howell, N. Gileadi, S. Tunyasuvunakool, K. Zakka, T. Erez, and Y. Tassa. Predictive sampling: Real-time behaviour synthesis with mujoco. *arXiv preprint arXiv:2212.00541*, 2022.
- [8] M. X. Authors. Mujoco xla (mjax), 2025. <https://mujoco.readthedocs.io/en/stable/mjx.html>.
- [9] G. Authors. Genesis: A universal and generative physics engine for robotics and beyond, December 2024. URL <https://github.com/Genesis-Embodied-AI/Genesis>.
- [10] V. Makoviychuk, L. Wawrzyniak, Y. Guo, M. Lu, K. Storey, M. Macklin, D. Hoeller, N. Rudin, A. Allshire, A. Handa, et al. Isaac gym: High performance gpu-based physics simulation for robot learning. *arXiv preprint arXiv:2108.10470*, 2021.
- [11] Y. Song and S. Ermon. Generative modeling by estimating gradients of the data distribution. *Advances in neural information processing systems*, 32, 2019.
- [12] Y. Song, J. Sohl-Dickstein, D. P. Kingma, A. Kumar, S. Ermon, and B. Poole. Score-based generative modeling through stochastic differential equations. *arXiv preprint arXiv:2011.13456*, 2020.
- [13] Y. Lipman, R. T. Chen, H. Ben-Hamu, M. Nickel, and M. Le. Flow matching for generative modeling. *arXiv preprint arXiv:2210.02747*, 2022.
- [14] M. Andrychowicz, A. Raichuk, P. Stańczyk, M. Orsini, S. Girgin, R. Marinier, L. Hussonot, M. Geist, O. Pietquin, M. Michalski, et al. What matters for on-policy deep actor-critic methods? a large-scale study. In *International conference on learning representations*, 2020.
- [15] L. Engstrom, A. Ilyas, S. Santurkar, D. Tsipras, F. Janoos, L. Rudolph, and A. Madry. Implementation matters in deep rl: A case study on ppo and trpo. In *International conference on learning representations*, 2019.
- [16] S. Feng, B. Burchfiel, T. Albina, and R. Tedrake. Tri’s robots learn new skills in an afternoon. here’s how, 2023. <https://medium.com/toyotaresearch/tris-robots-learn-new-skills-in-an-afternoon-here-s-how-2c30b1a8c573>.
- [17] G. R. Team, S. Abeyruwan, J. Ainslie, J.-B. Alayrac, M. G. Arenas, T. Armstrong, A. Balakrishna, R. Baruch, M. Bauza, M. Blokzijl, et al. Gemini robotics: Bringing ai into the physical world. *arXiv preprint arXiv:2503.20020*, 2025.

- [18] C. Chi, Z. Xu, C. Pan, E. Cousineau, B. Burchfiel, S. Feng, R. Tedrake, and S. Song. Universal manipulation interface: In-the-wild robot teaching without in-the-wild robots. *arXiv preprint arXiv:2402.10329*, 2024.
- [19] M. Posa, C. Cantu, and R. Tedrake. A direct method for trajectory optimization of rigid bodies through contact. *The International Journal of Robotics Research*, 33(1):69–81, 2014.
- [20] V. Kurtz, A. Castro, A. Ö. Öno, and H. Lin. Inverse dynamics trajectory optimization for contact-implicit model predictive control. *arXiv preprint arXiv:2309.01813*, 2023.
- [21] A. Aydinoglu, A. Wei, W.-C. Huang, and M. Posa. Consensus complementarity control for multi-contact mpc. *IEEE Transactions on Robotics*, 2024.
- [22] R. Rubinstein. The cross-entropy method for combinatorial and continuous optimization. *Methodology and computing in applied probability*, 1:127–190, 1999.
- [23] H. Xue, C. Pan, Z. Yi, G. Qu, and G. Shi. Full-order sampling-based mpc for torque-level locomotion control via diffusion-style annealing. *arXiv preprint arXiv:2409.15610*, 2024.
- [24] V. Kurtz. Hydrax: Sampling-based model predictive control on gpu with jax and mujoco mjx, 2024. URL <https://github.com/vincekurtz/hydrax>.
- [25] C. Pan, Z. Yi, G. Shi, and G. Qu. Model-based diffusion for trajectory optimization. *arXiv preprint arXiv:2407.01573*, 2024.
- [26] P. M. Wensing, M. Posa, Y. Hu, A. Escande, N. Mansard, and A. Del Prete. Optimization-based control for dynamic legged robots. *IEEE Transactions on Robotics*, 2023.
- [27] G. Williams, A. Aldrich, and E. A. Theodorou. Model predictive path integral control: From theory to parallel computation. *Journal of Guidance, Control, and Dynamics*, 40(2):344–357, 2017.
- [28] B. Vlahov, J. Gibson, M. Gandhi, and E. A. Theodorou. Mppi-generic: A cuda library for stochastic optimization. *arXiv preprint arXiv:2409.07563*, 2024.
- [29] Z. Wang, O. So, J. Gibson, B. Vlahov, M. S. Gandhi, G.-H. Liu, and E. A. Theodorou. Variational inference mpc using tsallis divergence. *arXiv preprint arXiv:2104.00241*, 2021.
- [30] H. J. T. Suh, T. Pang, and R. Tedrake. Bundled gradients through contact via randomized smoothing. *IEEE Robotics and Automation Letters*, 7(2):4000–4007, 2022.
- [31] Q. Le Lidec, F. Schramm, L. Montaut, C. Schmid, I. Laptev, and J. Carpentier. Leveraging randomized smoothing for optimal control of nonsmooth dynamical systems. *Nonlinear Analysis: Hybrid Systems*, 52:101468, 2024.
- [32] R. Gao, E. Hoogeboom, J. Heek, V. D. Bortoli, K. P. Murphy, and T. Salimans. Diffusion meets flow matching: Two sides of the same coin. 2024. URL <https://diffusionflow.github.io/>.
- [33] H. Zhu, T. Zhao, X. Ni, J. Wang, K. Fang, L. Righetti, and T. Pang. Should we learn contact-rich manipulation policies from sampling-based planners? *arXiv preprint arXiv:2412.09743*, 2024.
- [34] J. Bradbury, R. Frostig, P. Hawkins, M. J. Johnson, C. Leary, D. Maclaurin, G. Necula, A. Paszke, J. VanderPlas, S. Wanderman-Milne, and Q. Zhang. JAX: composable transformations of Python+NumPy programs, 2018. URL <http://github.com/google/jax>.
- [35] A. Handa, A. Allshire, V. Makoviychuk, A. Petrenko, R. Singh, J. Liu, D. Makoviichuk, K. Van Wyk, A. Zhurkevich, B. Sundaralingam, et al. Dextreme: Transfer of agile in-hand manipulation from simulation to reality. In *2023 IEEE International Conference on Robotics and Automation (ICRA)*, pages 5977–5984. IEEE, 2023.

- [36] J. Tobin, R. Fong, A. Ray, J. Schneider, W. Zaremba, and P. Abbeel. Domain randomization for transferring deep neural networks from simulation to the real world. In *2017 IEEE/RSJ international conference on intelligent robots and systems (IROS)*, pages 23–30. IEEE, 2017.
- [37] R. T. Rockafellar, S. Uryasev, et al. Optimization of conditional value-at-risk. *Journal of risk*, 2:21–42, 2000.
- [38] A. Dixit, M. Ahmadi, and J. W. Burdick. Risk-averse receding horizon motion planning for obstacle avoidance using coherent risk measures. *Artificial Intelligence*, 325:104018, 2023.
- [39] E. Perez, F. Strub, H. De Vries, V. Dumoulin, and A. Courville. Film: Visual reasoning with a general conditioning layer. In *Proceedings of the AAAI conference on artificial intelligence*, volume 32, 2018.
- [40] V. Kurtz and J. W. Burdick. Generative predictive control: Video summary, 2025. URL <https://youtu.be/mjL7CF8770w>.
- [41] C. D. Freeman, E. Frey, A. Raichuk, S. Girgin, I. Mordatch, and O. Bachem. Brax—a differentiable physics engine for large scale rigid body simulation. *arXiv preprint arXiv:2106.13281*, 2021.
- [42] A. Raffin, A. Hill, A. Gleave, A. Kanervisto, M. Ernestus, and N. Dormann. Stable-baselines3: Reliable reinforcement learning implementations. *Journal of Machine Learning Research*, 22 (268):1–8, 2021.
- [43] N. Fishman, L. Klarner, V. De Bortoli, E. Mathieu, and M. J. Hutchinson. Diffusion models for constrained domains. *Transactions on Machine Learning Research*, 2024.
- [44] N. Fishman, L. Klarner, E. Mathieu, M. Hutchinson, and V. De Bortoli. Metropolis sampling for constrained diffusion models. *Advances in Neural Information Processing Systems*, 36, 2024.
- [45] V. Kurtz and J. W. Burdick. Equality constrained diffusion for direct trajectory optimization. *arXiv preprint arXiv:2410.01939*, 2024.
- [46] M. Oquab, T. Darcet, T. Moutakanni, H. Vo, M. Szafraniec, V. Khalidov, P. Fernandez, D. Haziza, F. Massa, A. El-Nouby, et al. Dinov2: Learning robust visual features without supervision. *arXiv preprint arXiv:2304.07193*, 2023.
- [47] K. Zakka, B. Tabanpour, Q. Liao, M. Haiderbhai, S. Holt, J. Y. Luo, A. Allshire, E. Frey, K. Sreenath, L. A. Kahrs, C. Sferrazza, Y. Tassa, and P. Abbeel. Mujoco playground: An open-source framework for gpu-accelerated robot learning and sim-to-real transfer., 2025. URL https://github.com/google-deepmind/mujoco_playground.

A Appendix: Common SPC Algorithms

As discussed in Section 2.1, various SPC algorithms can be characterized by the weighting function $g(J)$. For instance, **MPPI** [6] uses a Boltzmann-like exponentially weighted average,

$$g_{MPPI}(J) = \exp(-J/\lambda), \quad (19)$$

where $\lambda > 0$ is the temperature parameter. A smaller λ give more weight to the lowest-cost samples.

In the low-temperature limit we recover **predictive sampling** [7],

$$g_{PS}(J) = \lim_{\lambda \rightarrow 0} \exp(-J/\lambda), \quad (20)$$

where the updated mean \bar{U} is simply chosen as the lowest-cost sample.

Another popular option is **CEM** [22, 5], which weighs the top performing samples equally,

$$g_{CEM}(J) = \begin{cases} 1 & \text{if } J \leq \gamma \\ 0 & \text{otherwise} \end{cases}. \quad (21)$$

The threshold γ is defined implicitly by a pre-defined number of *elite samples*. CEM is typically paired with an adaptive update rule for the variance of the proposal distribution.

Tsallis-MPPI [29] provides a middle ground between MPPI and CEM via a generalized exponential,

$$g_T(J) = \max(1 - (r - 1)J/\lambda, 0)^{\frac{1}{r-1}}, \quad (22)$$

where the original MPPI update is recovered as $r \rightarrow 1$.

High-performance implementations of these and other SPC algorithms are available in `hydrax` [24], a JAX-based SPC software package built on top of `MuJoCo MJX` [8].

Practical SPC performance relies heavily on dimensionality reduction via spline representations, e.g., representing $U = [u_0, u_1, \dots, u_T]$ with $T' \ll T$ knot points. While our implementation uses only the simplest zero-order-hold interpolation, the GPC framework is compatible with more sophisticated schemes such as Fourier features or higher-order splines [7].

B Appendix: Proof of Proposition 3

Proof. For simplicity of notation, we drop the conditioning on x and write the target distribution as $p_\sigma(U)$. We also denote the normal density as

$$q_U(\tilde{U}) \triangleq \mathcal{N}(\tilde{U}; U, \sigma^2).$$

The score of the target distribution is given by

$$\nabla_U \log p_\sigma(U) = \frac{\nabla_U p_\sigma(U)}{p_\sigma(U)}. \quad (23)$$

In the numerator we have

$$\nabla_U p_\sigma(U) = \frac{1}{\eta} \nabla_U \int q_U(\tilde{U}) g(\tilde{U}) d\tilde{U} \quad (24)$$

$$= \frac{1}{\eta} \int \nabla_U q_U(\tilde{U}) g(\tilde{U}) d\tilde{U} \quad (25)$$

$$= \frac{1}{\eta} \int q_U(\tilde{U}) \nabla_U \log q_U(\tilde{U}) g(\tilde{U}) d\tilde{U} \quad (26)$$

$$= \frac{1}{\eta} \mathbb{E}_{\tilde{U} \sim \mathcal{N}(U, \sigma^2)} \left[g(\tilde{U}) \frac{\tilde{U} - U}{\sigma^2} \right], \quad (27)$$

where η is a normalizing constant and we use the fact that $\nabla_U \log q_U(\tilde{U}) = (\tilde{U} - U)/\sigma^2$.

Bringing $1/\sigma^2$ outside the expectation, we have

$$\frac{\nabla_U p_\sigma(U)}{p_\sigma(U)} = \frac{\mathbb{E}_{\tilde{U} \sim \mathcal{N}(U, \sigma^2)} \left[g(\tilde{U})(\tilde{U} - U) \right]}{\sigma^2 \mathbb{E}_{\tilde{U} \sim \mathcal{N}(U, \sigma^2)} \left[g(\tilde{U}) \right]} \quad (28)$$

and thus the proposition holds. \square

C Appendix: Cosine-Distance Objective Weighting

We use a small modification of the flow matching loss based on the cosine similarity score

$$S_C(\mathbf{x}, \mathbf{y}) = \frac{\mathbf{x} \cdot \mathbf{y}}{\|\mathbf{x}\| \|\mathbf{y}\|}, \quad (29)$$

which measures directional similarity between vectors \mathbf{x} and \mathbf{y} . S_C outputs a scalar in $[-1, 1]$, with high values indicating a high degree of similarity.

In our case, we are more confident that the flow-matching objective \mathcal{L}_{GPC} (6) drives samples toward the true (but unknown) optimal action sequence U^* if the update $\bar{U}_k - \bar{U}_{k-1}$ and the flow target $\bar{U}_k - U_0$ are close. This is illustrated in the ‘‘flow matching’’ portion of Fig. 1. Darker shading indicates values of U_0 (typically drawn from a standard Gaussian) that are more informative. In particular, samples in the upper left-hand corner could be pushed toward \bar{U}_k but away from U^* , while samples in the lower right would flow in the correct direction.

To capture this mathematically, we define weights

$$w(\bar{U}_k, \bar{U}_{k-1}, U_0) = \exp(-\gamma(1 - S_C(\bar{U}_k - \bar{U}_{k-1}, \bar{U}_k - U_0))), \quad (30)$$

where the hyperparameter $\gamma > 0$ defines a decay rate as the two vectors move further apart (our implementation uses $\gamma = 2.0$). This gives us $w = 1$ if \bar{U}_{k-1} and U_0 are close in the cosine similarity sense, and $w \rightarrow 0$ as they move further apart. The final training loss is given by

$$w(\bar{U}_k, \bar{U}_{k-1}, U_0) \mathcal{L}_{GPC}(\theta; U_0; \bar{U}_k, x_k, t). \quad (31)$$

This modification is motivated by the fact that while the SPC update is a monte-carlo score ascent step, it does not obtain a true sample U^* from the optimal target distribution. In other words, \bar{U}_k is closer to an optimal sample than \bar{U}_{k-1} , but it is not the case that $\bar{U}_k = U^*$. This is an important distinction between the GPC setting and the typical generative modeling setting, where samples from the target distribution are freely available.

D Appendix: Domain Randomization Strategies

The availability of massively parallel simulators and the structure of the SPC/GPC paradigm enables a range of new DR possibilities. In particular, we can modify the SPC rollouts (4) by simulating each action sequence $U^{(i)}$ in several domains with randomized parameters (e.g., friction coefficients, body masses, etc.). This results in cost values indexed by both sample i and domain d , e.g.,

$$J^{(i,d)} = J(U^{(i)}; x_{k-1}, d). \quad (32)$$

We then aggregate this cost data across domains before performing the standard SPC update (5).

The simplest choice for aggregation would be take the average cost over all domains,

$$J^{(i)} = \mathbb{E}_d [J^{(i,d)}]. \quad (33)$$

This is analogous to the typical RL domain randomization framework, which considers the expected reward over all domains.

But the SPC/GPC framework allows for other possibilities as well. We can, for instance, take a more conservative approach and use the worst-case cost,

$$J^{(i)} = \max_d [J^{(i,d)}]. \quad (34)$$

Or we can use more sophisticated risk metrics like conditional value-at-risk (CVaR) [37, 38], which takes the expected cost in the $(1 - \beta)$ tail of the distribution:

$$J^{(i)} = \inf_{z \in \mathbb{R}} \mathbb{E}_d \left[z + \frac{\max(J^{(i,d)} - z, 0)}{1 - \beta} \right], \quad (35)$$

	Pendulum	Cart-Pole	Double Cart-Pole	Push-T	Walker	Crane	Humanoid
DoFs	1	2	3	5	9	7	29
Num. actuators	1	1	1	2	6	3	23
Observation Size	3	5	8	5	18	23	56
Planning horizon (s)	0.5	1.0	0.8	0.5	0.6	0.8	0.9
Planning knots	5	10	10	5	4	2	3

Table 2: Example task specification parameters.

where $\beta \in [0, 1]$ determines the degree of risk sensitivity.

These and other risk strategies for online domain randomization are implemented in `hydrax` [24], making them readily available for both GPC training and online deployment in a bootstrapped SPC controller. Section 6.3 illustrates the impact of different domain randomization strategies on the luffing crane example.

E Appendix: Example System Details

Details regarding each of the example systems from Section 6 can be found below, with further details in Table 2. We represent the action sequence U with a zero-order-hold spline over a fixed number of knot points. Using few knot points is critical for good SPC performance, particularly on the higher-DoF examples.

Inverted pendulum: This simple one-dimensional system requires swinging a pendulum to the upright position and balancing it there. Torque limits prevent the pendulum from swinging directly upright: the policy must gradually pump energy into the system. The observation $y = h(x)$ consists of sine and cosine of the angle, along with angular velocity.

Cart-pole: An unactuated pendulum is mounted on an actuated cart. Control actions are torques applied to the cart, and the task is to balance the pendulum upright. While this is a relatively simple nonlinear system, obtaining successful human demonstrations would be difficult. The observations are sine and cosine of the pendulum angle, position of the cart, and linear and angular velocities.

Double cart-pole: In this extension of the cart-pole example, an unactuated double pendulum is mounted on the cart. The fast and chaotic double pendulum dynamics make this task particularly challenging. As for the cart-pole, observations include sine and cosine of pendulum angles, cart position, and linear and angular velocities.

Push-T: A robotic finger pushes a T-shaped block to a goal position and orientation on a table. This task has been solved with behavior cloning [1], and is a standard example of a task that requires multi-modal reasoning. The observations include pusher position, block position, and block orientation.

Planar biped: A robot walker, constrained to the sagittal plane, is tasked with moving forward at 1.5 m/s. The high dimensionality of this system would make teleoperation for behavior cloning difficult. Successful locomotion also requires fast replanning. The observation is the full system state (positions and velocities), excluding the horizontal position.

Luffing crane: A swinging payload is attached via a rope to a luffing crane. Control actions are target boom angles and rope length. This underactuated system provides a particularly useful testbed for investigating the impact of modeling errors and domain randomization strategies. The observation includes crane joint angles and the position and velocity of the payload relative to the target.

Humanoid standup: A Unitree G1 humanoid model is tasked with reaching a standing configuration. Initial conditions are random joint angles, joint velocities, and base orientation, so that the robot begins sprawled on the ground. The observation includes all joint angles and joint velocities, floating base velocity, floating base position, and floating base orientation relative to the upright.

	Pendulum	Cart-Pole	Double Cart-Pole	Push-T	Walker	Crane	Humanoid
Architecture	MLP	MLP	MLP	CNN	CNN	CNN	CNN
Iterations	10	10	50	20	20	10	20
Train (min:sec)	00:30	01:20	17:10	17:30	9:36	6:15	113:18
Envs. (N_E)	128	128	256	128	128	512	128
SPC samp. (N_S)	8	8	16	128	16	4	32
Policy samp. (N_P)	2	2	16	32	16	2	32
Episode len. (sec)	4.0	2.0	4.0	4.0	5.0	5.0	8.0
Num. Params.	1541	5898	20362	19990	49768	48680	368567
Batch size	128	128	128	128	128	1024	128
Learning rate	10^{-3}	10^{-3}	10^{-3}	10^{-3}	10^{-3}	10^{-3}	10^{-3}
Epochs	10	100	10	10	10	20	10
Inference (ms)	1.0	1.3	1.3	3.8	8.1	2.4	4.0
ODE step size δt	0.1	0.1	0.1	0.1	0.1	0.1	0.1
Ctrl. Freq. (Hz)	50	50	50	50	50	30	50

Table 3: Summary of training and inference hyperparameters.

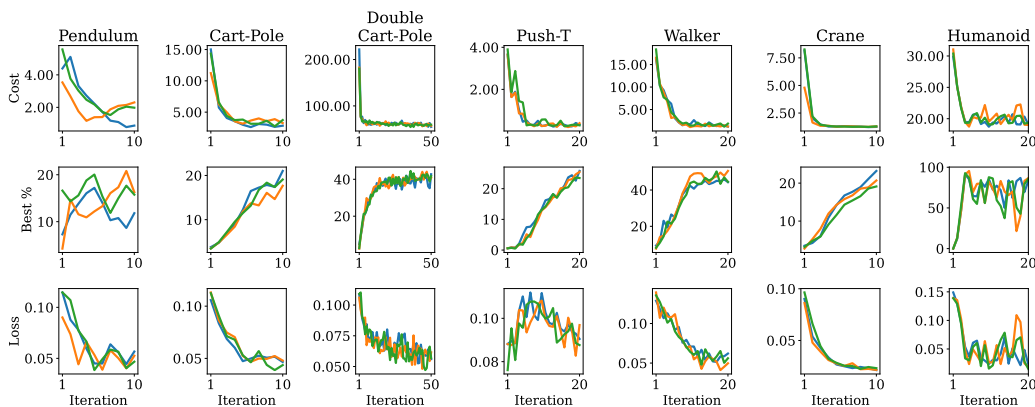


Figure 5: Training curves showing the average cost J , percent of states in which the flow-matching policy generated the best action sequence, and the loss \mathcal{L}_{GPC} from three random seeds. GPC is able to leverage the training stability of supervised learning while avoiding the need for demonstrations.

F Appendix: Training Details

Hyperparameters for policy training and inference are shown in Table 3. When evaluating a trained SPC or GPC+ policy, we used a total of 128 simulation rollouts. For SPC, all of these are drawn from a Gaussian proposal distribution. For GPC+, 64 are from the Gaussian distribution and 64 are from the flow matching policy.

The hyperparameters in Table 3 are not highly optimized: our primary objective is merely to confirm the ability of GPC to train usable generative policies. We leave a systematic study of the relative impact of various hyperparameters for future work.

Training curves for each of the examples are shown in Fig. 5. In addition to the average loss and average cost at each iteration, we plot the percent of states in which the flow-matching policy generates the lowest-cost action sequence. Recall that some samples come from the policy, while others come from the SPC normal proposal distribution (Algorithm 1, lines 6-7). A higher percentage of best samples coming from the policy is a useful indicator of policy performance, and tends to increase (modulo noise from randomized initial conditions) throughout the training process.

Interestingly, this percentage does not reach 100%, even after many iterations. This is due to the fact that a good sample from the policy also improves SPC performance at the following time step, since a good policy sample at step $k - 1$ shifts the mean of the proposal distribution at step k close to optimality.